SVU-International Journal of Engineering Sciences and Applications (2025) 6(1): 1-8
Print ISSN 2785-9967 | Online ISSN 2735-4571
DOI 10.21608/svusrc.2024.297015.1220

Artificial Neural Networks-Based Energy Storage Predictor of $(Ba_{0.85}Ca_{0.15})(Ti_{0.9}Zr_{0.1})O_3$ under Temperature-Induced Variation

Dina A. Naser [1,*], Mohamed H. Essai Ali [2], Abd El-Razek Mahmoud [3], and G. A. Gamal [3]

Abstract Comprehending and predicting the fluctuations in the energy storage functionality of ferroelectric-based apparatuses throughout a broad range of temperatures is crucial. To achieve this, we developed and simulated a Function Fitting ANN model using MATLAB. The model was trained using the back-propagation algorithm, effectively capturing the relationship between the applied electric field, and resulting polarization through experimental data. The model demonstrates excellent performance with two hidden layers consisting of 37 neurons in each and three input layers. Extensive experimentation confirms the model's impressive accuracy in predicting energy storage performance, particularly at different temperature conditions around Curie temperature Tc. The experimental part of the study was done in the temperature range (43-95 °C) which seems to be limited. However, it justifies temperature-induced changes around the Curie temperature (T_C). Above curie temperature ($T > T_C$), the material becomes paraelectric and loses its spontaneous polarization resulting in more decrease in recoverable energy-storage density and efficiency. The remarkable predictive performance of the model is attributed to its remarkably low mean square error of 3.68×10^{-5}. This result emphasizes the model's precision and reliability in accurately forecasting energy storage parameters. Finally, BCZT ceramic samples were selected for the present work for being a very famous ferroelectric material and has well-known ferroelectric properties.

Keywords: Artificial Neural Networks; Energy Storage Parameters; Ceramic Capacitors; Temperature Variation; Ferroelectric Hysteresis Loops.

1 Introduction

Energy storage materials play a vital role in various applications, including capacitors, sensors, and energy harvesting devices. The main importance of energy storage in capacitance lies in its ability to store and release electrical energy quickly. Capacitors are commonly used in power electronics and electrical systems to provide short bursts of energy. They can deliver high power quickly, making them crucial for applications needing high-speed energy storage and release [1].

BCZT is an exceptional piezoelectric ceramic composed of a perovskite structure commonly known as ABO3 [2]. Due to its remarkable properties, including a high Curie temperature and strong ferroelectricity, BCZT has garnered significant interest as a suitable material for a range of technological advancements. However, its behavior at different temperature conditions, particularly the temperature-induced variations on the (P-E) hysteresis loop, is studied [3-5].

Temperature variations, however, impose significant challenges on the energy storage behavior of BCZT. The PE hysteresis loop, representing the relationship between polarization and electric field, undergoes dynamic changes due to thermal effects. Understanding and predicting these variations is essential to ensure the reliable operation of BCZT-based devices across a wide temperature range. It can also explain how the material's properties change at the effect of temperature. This is crucial for optimizing their design and efficiency. Using ANNs presents an advantageous solution for researchers grappling with the unwanted electrical spark in their samples. This challenge can significantly face the progress and effectiveness of scientific progress.

The literature survey revealed the difficulty of comparison with other models. This is due to:

-Traditional modeling approaches often struggle to capture the nonlinear and complex nature of the P-E hysteresis loop [7,8]. An example of modeling and simulation of a hysteresis loop under the influence of temperature variation can be seen in references [9-11].

- Other studies might use different architectures or additional techniques to ensure better generalization across various results.

Received: 12 June 2024/ Accepted: 28 September 2024
* Corresponding Author: Dina A. Naser, dinaabdenaser29@gmail.com
Mohamed H. Essai Ali, mhessai@azhar.edu.eg
Abd El-Razek Mahmoud, abdelrazek.mahmoud@sci.svu.edu
G. A. Gamal, gamal.elkareem@sci.svu.edu.eg
1. High Institute of Engineering &Technology Luxor- Tod, Luxor, Egypt
2. Faculty of Engineering, Al-Azhar University, Qena, Egypt
3. Faculty of Science, South Valley University, Qena, Egypt

- The proposed model demonstrates superior performance especially in the test area compared to previously reported ANN-based approaches [6]. Additionally, traditional modeling methods include the ferromagnetic Jiles Atherton and the Neuroevolutionary or mathematical models in Refs. [7,8,11] have shown shortcomings in capturing the complete curve. In contrast, the proposed model exhibits a key advantage: its ability to predict a complete hysteresis loop even at non-standard temperatures, a capability absents in prior methods.
It must be noted that this research applies a novel approach by using Artificial Neural Networks (ANNs) to predict energy storage characteristics.

Machine learning is generally used in the prediction of descriptors for ferroelectricity [12,13]. However, Future research could explore the development of comprehensive ANN models that can simultaneously predict and simulate ferroelectric hysteresis loops [14].

This study showcases the strength of (ANNs) by demonstrating their ability to learn the data behavior and establish accurate correlations. ANNs have the potential to surpass the limitations of traditional models, allowing for enhanced predictions of energy storage performance across diverse temperatures.

The framework presented in this research involves training ANNs on a comprehensive dataset, which includes (P-E) hysteresis loops of BCZT at various temperatures and constant electric fields. By providing input variables like temperature, electric field strength, and time to these ANNs, we can obtain precise predictions of hysteresis loops, which can subsequently be used to measure energy storage parameters.

2 Methodology

2.1 BCZT powder synthesis

BCZT ceramic samples were successfully produced in ambient air via the solid reaction method. The process involved weighing and mixing $BaCO_3$(99.999.9999 Sigma Aldrich), $CaCO_3$ (99.99% Sigma Aldrich), ZrO_2 (99.99% Sigma Aldrich), and TiO_2 (99.999% Sigma Aldrich), according to the desired composition formula. After milling and mixing in ethanol for 24 hours, the mixture was dried at 80°C for 4 hours and then sieved. Thermal calcination was conducted in an electric digitalized furnace (type KSL-1700x) at 1300°C for 2 hours in an air atmosphere to avoid contamination. The calcined powder was mixed with 5 wt% polyvinyl alcohol (PVA) binder, pressed into pellets, and sintered at 1550°C for 4 hours.

2.2 Description of dataset

In this work, the dynamic ferroelectric hysteresis data (mono P-E loops) was measured from single-crystal BCZT. The used BCZT single crystal was of tetragonal {001} phase. Rigorous characterization techniques, including XRD and SEM, were reported in a previous paper [15], The hysteresis loops were measured with a frequency of 50 Hz and field amplitude of 25 kV/cm, where the BCZT disc-shaped plates with an area of 0.54 cm^2 and thickness of 850 µm. A constant electric field (25 kV/cm) was used in the BCZT study for many reasons: a) To explore the effect of hysteresis loops against temperature variation and hence energy storage behavior. b) The model's accuracy depends on the quality and quantity of the experimental data used for training. The 25 kV/cm is used to obtain (from the experimental work experience) a large amount of data points which is required for energy storage work. This value is convenient to avoid the electrical breakdown in the BCZT sample. The ferroelectric properties and Rayleigh analysis of the BCZT ceramics sample were measured using (Precision 10 kV HVI-SC Radiant Ferroelectric Technologies Inc.).

2.3 Artificial neural network for energy storage parameters prediction

The energy storage prediction model utilizes a Function Fitting Neural Network in the MATLAB program, offering flexibility to capture intricate, non-linear relationships within the data. To study temperature-induced variations in hysteresis loops, multiple curves were employed for training, presenting a challenge due to repetitive electrical field values. This complexity was mitigated by designing the input layer with time, instantaneous electrical field, and temperature variables. The dataset was split into training, validation, and testing sets (in a ratio of 0.8:0.1:0.1), and an ANN architecture with one input layer and two hidden layers, each containing 37 neurons, was implemented. **Fig. 1** represents the Artificial neural network model. Backpropagation and sigmoid activation functions facilitated training, while the Bayesian regularization algorithm optimized weights and biases, refining predictions iteratively. By minimizing mean square error, the network continuously improved accuracy. Calculation of energy storage coefficients relies on mathematical operations applied to hysteresis loops from ferroelectric analysis. **Table 1** provides a summary of the

characteristic training values.

Table 1 Training characteristics of ANN

ANN Characteristics	Value/ Description
Neural network function	Function-fitting neural network
Number of input layers	3
Number of output layers	1
Number of hidden layers	2
Number of neurons in each hidden layer	27
Number of weight elements	892
Input Weights	{3×1 cell array of 1 weight}
Layer Weights	{3×3 cell array of 2 weight}
Division function	dividing division function
Hidden layers activation function	Hyperbolic sigmoid function (logsig)
Output layer activation function	Linear transfer function (purelin)
Training algorithm	Bayesian regularization backpropagation (trainbr)
Error performance function	Mean squared error
Learning rate parameter	5

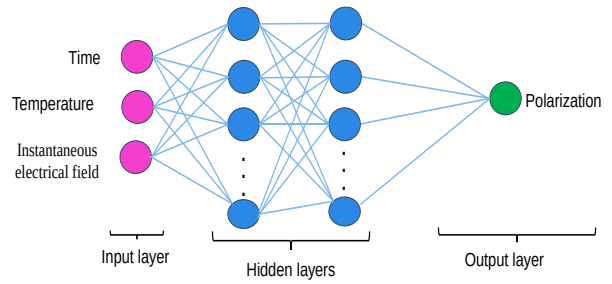

Fig. 1 Artificial neural network model

2.4 Measurement of predicted energy storage parameters

The performance of energy storage, determined from the unipolar (P–E) hysteresis loop, is assessed using the following key parameters:

Recoverable Energy Storage Density (W_{rec}): This parameter measures the energy that can be retrieved per unit volume and is generally calculated as in Eq. (1):

$$w = \int_{p_r}^{p_{max}} EdP \qquad (1)$$

Here, the integration extends from the remanent polarization (P_r) to the maximum polarization (Pmax) along the lower segment of the loop.Energy Storage Efficiency (η): This represents the proportion of released electrical energy to the stored electrical energy, indicating the efficiency of the charge/discharge process. It can be calculated using Eq. (2):

$$\eta = W_{rec}/W_{total} \qquad (2)$$

denotes the energy storage density during the charging process only.

Effective Capacitance (C_{max}): This is determined at the maximum unipolar measurement voltage and can be derived from P_{max} using Eq. (3). Effective capacitance (nF) at the maximum mono measurement voltage is derived from P_{max} by:

$$C_{max} = (P_{max} \times 1000 \times Area)/(max.Volts) \qquad (3)$$

3 Results and Analysis

3.1 Ferroelectric analysis

The effect of the variation of the electric field against the polarization of BCZT at random temperature (43-95°C) is depicted in **Fig. 2**. The figure shows the hysteresis mono loops behavior as a function of the polarization-dependent electric field at constant electric field strength 25 kV/cm and random temperature of BCZT sample. The well-saturated loops are strongly temperature dependent. As observed, a slim hysteresis loop has been detected at lower applied fields attributed to polar nano-regions contribution and nano-domains. while the ferroelectric hysteresis curve becomes broader, indicating a greater energy loss during the polarization-switching process [13,16]. The values of remnant polarization and maximum polarization at 25 kV/cm and different temperatures are shown in **Fig. 2**, Both the remnant polarization and the maximum polarization are nearly constant until reaching 75°C then they increase gradually with the increase of temperature.

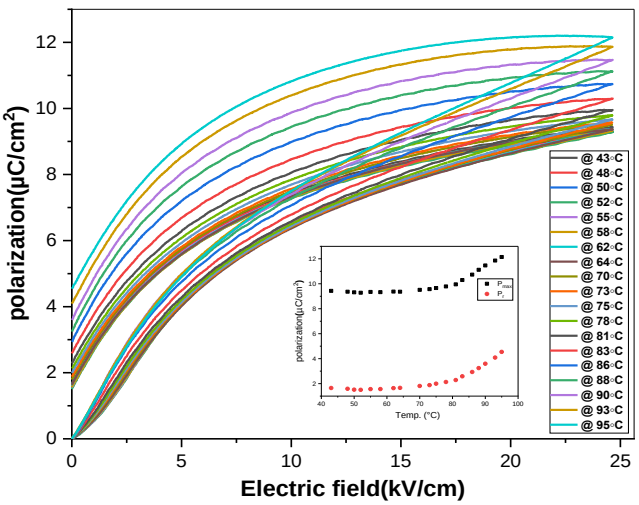

Fig. 2 Mono (P-E) hysteresis loops for BCZT sample at 25 kV/cm and different temperatures. Inside the figure, the maximum, and remnant polarization of BCZT relative to

temperature

3.2 Energy storage parameters of experimental data

Temperature dependence of recoverable energy-storage density, efficiency, and maximum effective capacitance of BCZT at electric field strength 25kV/cm are shown in **fig.3**. In **fig.3(a, b)** below Curie Temperature (T_C < 91.7) BCZT ferroelectric exhibit a spontaneous polarization due to the alignment of dipoles. This results in a slight increase in recoverable energy-storage density and efficiency (same behavior). Approaching and around Curie temperature (T ≃ T_C), as the temperature approaches the Curie temperature, the ferroelectric material undergoes a phase transition from a ferroelectric phase Tara electric phase reducing the spontaneous polarization and leading to a decrease in recoverable energy-storage density and efficiency. This reduction is a consequence of the decreasing order in the material as it transitions to a state with less inherent polarization. Above curie temperature (T > T_C), the material becomes paraelectric and loses its spontaneous polarization resulting in more decrease in recoverable energy-storage density and efficiency. In **Fig. 3c** below curie temperature (T < T_C) due to increasing polarization and alignment of dipoles a slight decrease in the dielectric constant and effective capacitance. As the temperature approaches T_C and beyond it, the spontaneous polarization increases, leading to a slight increase in the dielectric constant and effective capacitance.

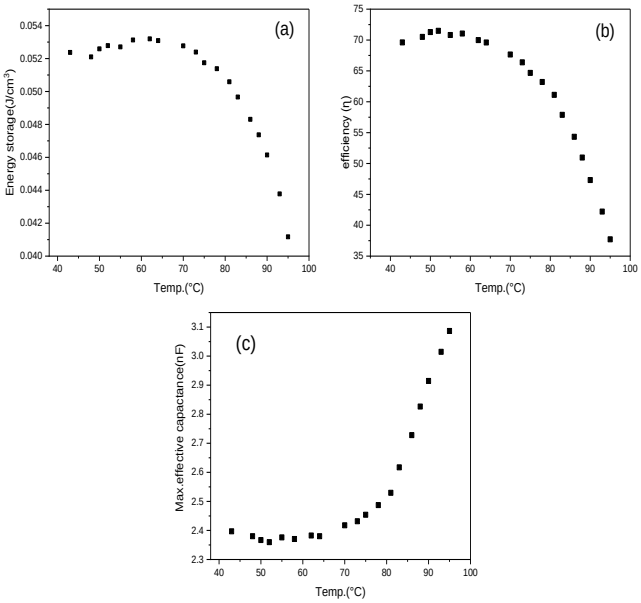

Fig. 3 (a) Temperature dependence of recoverable energy-storage density. (b) The efficiency of BCZT at 25kV/cm versus temperature (c) Maximum effective capacitance versus temperature

3.3 Training performance of ANN using a ferroelectric data set

The relationship between predicted values (outputs) and actual values (targets) generated by a trained Artificial Neural Network (ANN) across training, validation, and testing datasets, along with a combined regression plot is shown in **Fig. 4**. The dashed line represents the theoretical ideal scenario where the calculated outputs perfectly align with the targets (Y=T), forming a 45-degree angle. Outlying data points are discernible via the scatter plot. Moreover, a solid line denotes the linear regression line that optimally fits the relationship between outputs and targets.

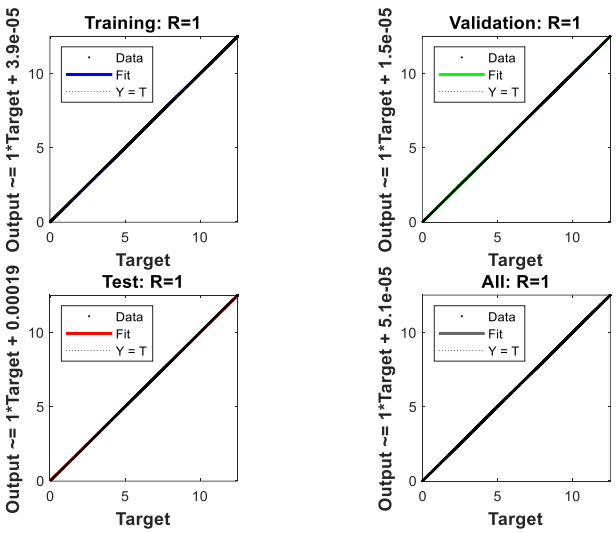

Fig. 4 The regression plot of ANN

The R-value, serving as the correlation coefficient, quantifies the strength and direction of the linear association between calculated output values and corresponding target values. A maximum R-value of 1 denotes a flawless correlation between output and target values. Remarkably, an R-value of 1 was observed across the training, validation, and testing regression sets. Consistent with the recommended acceptance criterion within the MATLAB neural network toolbox, an R-value of 0.9 is deemed satisfactory. Such a level of fit indicates proficient training, validation, and testing, signifying robust generalization without overfitting. Ideally, all scatterplot dots would precisely align along the diagonal line, indicative of a near-perfect alignment between predicted and actual values. The mean square error (MSE) is a commonly used metric in neural networks to assess the accuracy of predictions. It can be measured by eq:

$$MSE = (1/n) \times \sum (Y-T)^2 \qquad (4)$$

Where n is the number of samples in the dataset. In the present ANN, it has a small value equal to 3.68×10^{-5}. MSE value indicates better performance, as it means that the model's predictions are closer to the actual values.

Fig. (5,6) shows the performance graph and the training state of the developed fitting network. It is seen in the graph that the lines drawn with the data obtained from the training, validation, and test stages of ANN intersect with the best value shown with dotted lines in the 2000th epoch. The termination of the training phase of the ANN by reaching the lowest MSE value indicates that the training of the model is ideally completed. It is important to analyze the error histogram graphs in making the performance analysis of ANNs. In the error histogram graphs, the error rates between the output values obtained from ANN and the target values are shown on the graph. Examining the error histogram graph in **Fig.7.**

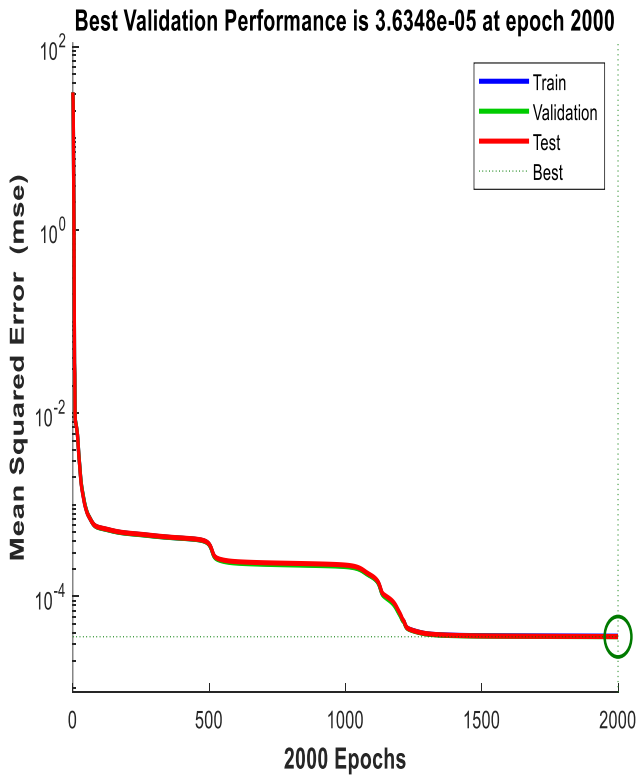

Fig. 5 Performance of the ANN model for training, validation, and testing data

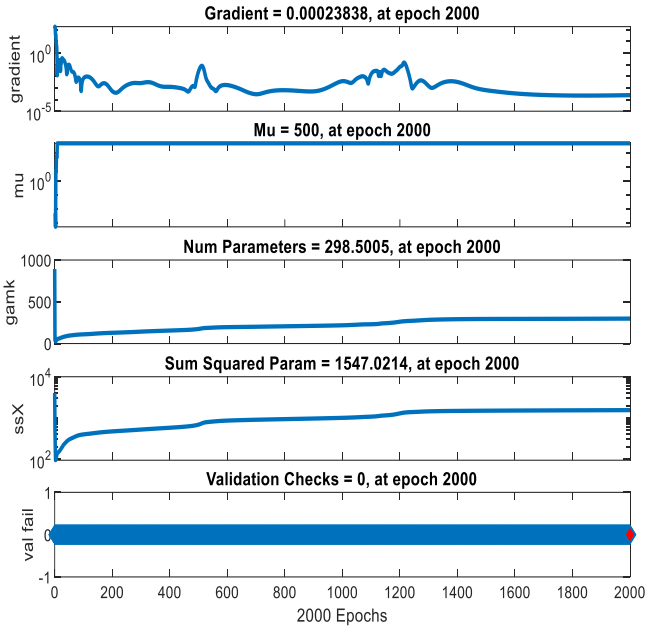

Fig. 6 Performance of selected ANN model in terms of gradient, mu, ssx, gamk, and validation fail parameter

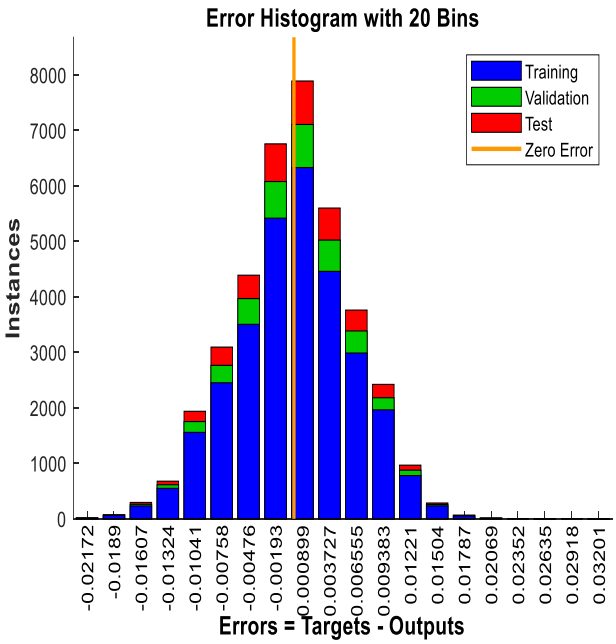

Fig.7 The error histogram for ANN

3.4 Comparison of predicted and actual data

The comparison between the predicted and experimental relationship between electric field and polarization at constant electric field strength 25 (kV/cm) and different temperature ranges (43-95 °C) is illustrated in **Fig. 8**. Temperature range seems to be limited; however, it justifies temperature-induced changes around the Curie temperature (Tc). Above curie temperature ($T > T_C$), the material becomes paraelectric and loses its spontaneous polarization resulting in a decrease in recoverable energy-storage density and efficiency. As for **Fig. 8,** the presented comparative analysis reveals a congruent and flawless alignment in the P-E hysteresis loops between the experimental and predicted datasets. This concordance not only imparts valuable insights but also substantiates the precision of the ANN employed. It attests to a profound comprehension of the material's characteristics. The perfection in matching signifies that the ANN model utilized for predicting the hysteresis loop encapsulates all pertinent parameters and their interrelations.

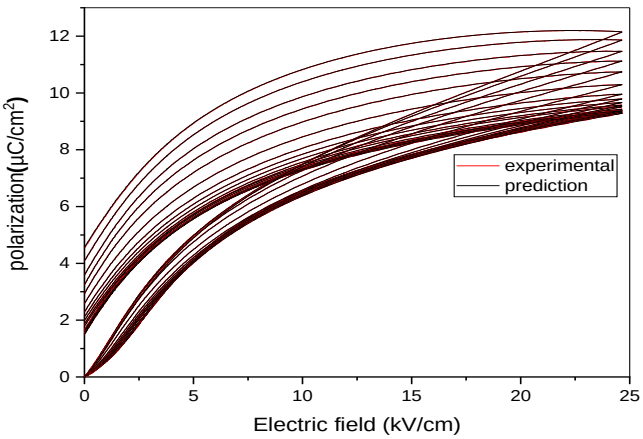

Fig. 8 Comparison between experimental and prediction mono (P-E) loops of BCZT at 25 (kV/cm) electric field and random temperature (43-95 °C)

Fig. 9 represents a comparison between experimental values and predictive values for energy storage parameters including recoverable energy storage density (a), efficiency (b), and maximum effective capacitance(c) under temperature variations. The figure indicates the model's reliability in predicting performance changes due to temperature variations. However, some correspondence in the overall behavior of the material, and this apparent discrepancy in the position of the points may be a result of differences in precision between the calculation accuracy of the software that generates its calculations.

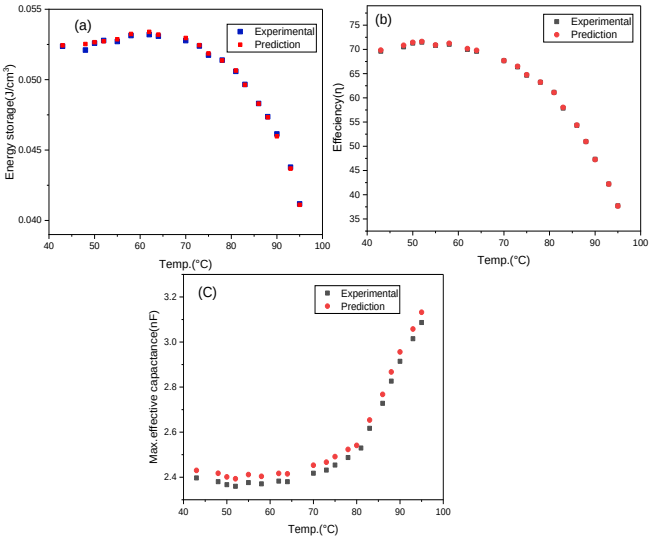

Fig. 9 Comparison between experimental and prediction data of (a) Recoverable energy storage (b) Efficiency (c) Maximum effective capacitance of BCZT versus temperature range (43-95 °C)

3.5 Prediction of (P-E) hysteresis loop under temperature variation

The predictive methodology for (P-E) hysteresis loops in this study relies on forecasting these loops within a temperature range encompassing and beyond the experimental temperature. This approach ensures the network's ability to discern variations in shape both preceding and succeeding the Curie temperature. **fig.10(a, b)** shows the predicted mono (P-E) loops of BCZT at 25 (kV/cm) electric field and random temperature before and after Tc. Due to the effective training of the ANN, it has demonstrated proficiency in distinguishing changes in curves with response to temperature variations. This appears in Fig. 10a where the curves exhibit a slender configuration, contrasting with their broader configuration in Fig. 10b.

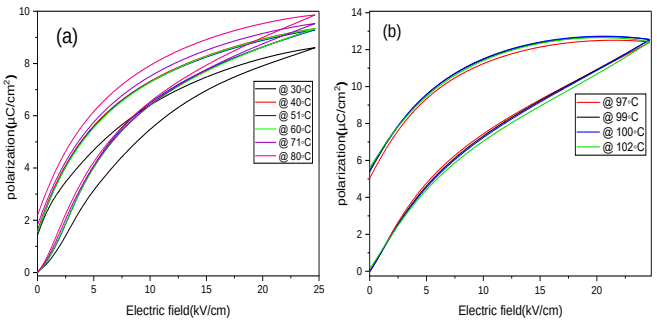

Fig.10 (a) Predicted mono (P-E) loops of BCZT at 25 (kV/cm) electric field and random temperature before T_c. (b) Prediction of

mono (P-E) loops of BCZT at 25 (kV/cm) electric field and random temperature after T_c

3.6 Behavior of Predicted Energy Storage Parameters

Utilizing eqs. (2, 3, 4), energy storage parameters for the predicted monodomain (P-E) loops of (BCZT) are computed, and these parameters are graphically represented versus temperature in **Fig. 11**. Remarkably, the trends observed in the recovered energy storage density and efficiency from the predicted data closely parallel those obtained experimentally beyond and before T_c.

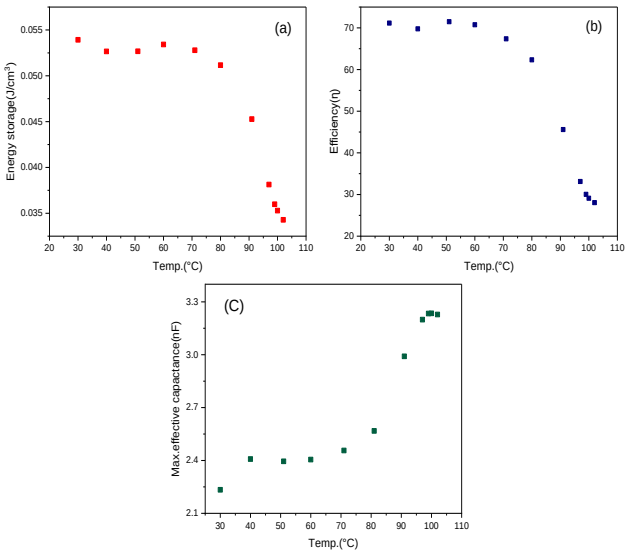

Fig. 11 (a, b) Energy storage parameters for predicted data of mono (P-E) loops 25 (kV/cm) of BCZT versus temperature. (c) Maximum effective capacitance for predicted data of mono (P-E) loops 25 (kV/cm) of BCZT

7 Conclusion

- In conclusion, this research aimed to explore the potential of Artificial Neural Networks (ANNs) in accurately forecasting energy storage parameters. Especially for ($Ba_{0.85}Ca_{0.15}$) ($Ti_{0.9}Zr_{0.1}$) O_3 (BCZT) ferroelectric materials at different temperature conditions.
- The research addresses an important topic in the field of ferroelectric materials and energy storage.
- Through extensive experimentation and data analysis, it was observed that ANN can effectively capture the complex relationship between temperature-induced variations and the hysteresis loops of the BCZT material through extensive testing.
- By employing the function fitting technique of ANN, we successfully modeled the ferroelectric hysteresis mono-loop of BCZT in the scope of the temperature range (30:102 °C).
-This allowed us to develop an accurate and efficient model for estimating the energy storage parameters based on the predicted hysteresis loops. These findings highlight the capability of ANNs to capture intricate relationships inherent in ferroelectric material properties and energy storage. Thereby solidifying their potential as robust prediction tools within this research domain.
- This research can lead to improved reliability, enhanced power management, predictive maintenance, and material optimization for diverse electronic applications
- Future studies might explore alternative network architectures or techniques like dropout regularization to promote better model generalization across diverse operating conditions.
- For generalization, the application of ANN and predicting energy storage can be expanded to other types of ferroelectric materials like relaxors or anti-ferroelectrics**.**

References

[1] Shkuratov, Sergey I., and Christopher S. Lynch. "A review of ferroelectric materials for high power devices." Journal of Materiomics 8.4 (2022): 739-752 https://doi.org/10.1016/j.jmat.2022.04.002.
[2] Li, Wei, et al. "Structural and dielectric properties in the (Ba1−xCax)(Ti0. 95Zr0. 05) O3 ceramics." Current Applied Physics 12.3 (2012): 748-751 https://doi.org/10.1016/j.cap.2011.10.013
[3] Shi, Jing, et al. "Effects on structure and properties of BCZT lead-free piezoelectric ceramics by rare-earth doping." Ferroelectrics 507.1 (2017): 186-197 https://doi.org/10.1080/00150193.2017.1283941
[4] Lakouader, Afaak, et al. "Improved energy storage and electrocaloric properties of lead-free Ba0. 85Ca0. 15Zr0. 1Ti0. 9O3 ceramic." Journal of Materials Science: Materials in Electronics 33.18 (2022): 14381-14396 https://doi.org/10.1007/s10854-022-08362-y
[5] Hanani, Zouhair, et al. "Structural, dielectric, and ferroelectric properties of lead-free BCZT ceramics elaborated by low-temperature hydrothermal processing." Journal of Materials Science: Materials in Electronics 31 (2020): 10096-10104. https://doi.org/10.1007/s10854-020-03555-9
[6] Yekta, Parastoo Vahdati, Farzad Jaafari Honar, and Mohammad Naghiyan Fesharaki. "Modelling of hysteresis loop and magnetic behaviour of Fe-48Ni alloys using artificial neural network coupled with genetic algorithm." Computational Materials Science 159 (2019): 349-356. https://doi.org/10.1016/j.commatsci.2018.12.025
[7] Alhmoud, Lina, et al. "Prediction of Hysteresis Loop of Barium Hexaferrite Nanoparticles Based on Neuroevolutionary Models." Symmetry 13.6 (2021): 1079. https://doi.org/10.3390/sym13061079
[8] Ma, Zhi, et al. "Modeling of hysteresis loop and its applications in ferroelectric materials." Ceramics International 44.4 (2018): 4338-4343. https://doi.org/10.1016/j.ceramint.2017.12.027
[9] Al Janaideh, Mohammad, Mohammad Al Saaideh, and Micky Rakotondrabe. "Temperature dependent hysteresis modeling of a piezotube actuator using elman neural network." Dynamic

Systems and Control Conference. Vol. 59148. American Society of Mechanical Engineers, 2019. https://doi.org/10.1115/DSCC2019-9184

[10] Tabaza, T. A., et al. "Hysteresis modeling of impact dynamics using artificial neural network." Journal of Mechanics 37 (2021): 333-338 https://doi.org/10.1093/jom/ufab007.

[11] Bai, Yang, et al. "Simulation and validation of temperature-dependent ferroelectric properties of multifunctional BCZT and KNBNNO ceramics." Materials Research Express 5.11 (2018): 116305 DOI: 10.1088/2053-1591/aade7b.

[12] He, Jingjin, et al. "Machine learning identified materials descriptors for ferroelectricity." Acta Materialia 209 (2021): 116815 https://doi.org/10.1016/j.actamat.2021.116815

[13] Shen, Zhong-Hui, et al. "Machine learning in energy storage materials." Interdisciplinary Materials 1.2 (2022): 175-195 https://doi.org/10.1002/idm2.12020

[14] Laosiritaworn, Wimalin S., Rattikorn Yimnirun, and Yongyut Laosiritaworn. "Artificial neural network modeling of ferroelectric hysteresis: An application to soft lead zirconate titanate ceramics." Key Engineering Materials 421 (2010): 432-435 https://doi.org/10.4028/www.scientific.net/KEM.421-422.432

[15] Elkelany, Essam A., et al. "New insights into the effect of glass addition on the piezoelectric and thermal stability properties of (Ba0. 85Ca0. 15)(Ti0. 9Zr0. 1) O3 Pb-free ceramic by defect engineering of MPB." Ceramics International 49.23 (2023): 38305-38317. https://doi.org/10.1016/j.ceramint.2023.09.163

[16] Hanani, Zouhair, et al. "Thermally stable high energy storage performances and large electrocaloric effect over a broad temperature span in lead-free BCZT ceramic." RSC advances 10.51 (2020): 30746-30755. DOI: 10.1039/D0RA06116F